



OPEN ACCESS

EDITED BY

Mario Cunha,
University of Porto, Portugal

REVIEWED BY

Dinesh Fernando,
Swedish University of Agricultural Sciences,
Sweden
Jinbo Shen,
Zhejiang Agriculture and Forestry
University, China

*CORRESPONDENCE

Hugo Germain
✉ hugo.germain@uqtr.ca

RECEIVED 19 July 2023

ACCEPTED 04 September 2023

PUBLISHED 22 September 2023

CITATION

Sanchez Carrillo IB, Hoffmann PC, Barff T,
Beck M and Germain H (2023) Preparing
Arabidopsis thaliana root protoplasts for
cryo electron tomography.
Front. Plant Sci. 14:1261180.
doi: 10.3389/fpls.2023.1261180

COPYRIGHT

© 2023 Sanchez Carrillo, Hoffmann, Barff,
Beck and Germain. This is an open-access
article distributed under the terms of the
[Creative Commons Attribution License
\(CC BY\)](https://creativecommons.org/licenses/by/4.0/). The use, distribution or
reproduction in other forums is permitted,
provided the original author(s) and the
copyright owner(s) are credited and that
the original publication in this journal is
cited, in accordance with accepted
academic practice. No use, distribution or
reproduction is permitted which does not
comply with these terms.

Preparing *Arabidopsis thaliana* root protoplasts for cryo electron tomography

Ingrid Berenice Sanchez Carrillo¹, Patrick C. Hoffmann²,
Teura Barff¹, Martin Beck^{2,3} and Hugo Germain^{1*}

¹Department of Chemistry, Biochemistry, and Physics, Université du Québec à Trois-Rivières, Trois-Rivières, QC, Canada, ²Department of Molecular Sociology, Max-Planck-Institute for Biophysics, Frankfurt, Germany, ³Institute of Biochemistry, Goethe University Frankfurt, Frankfurt, Germany

The use of protoplasts in plant biology has become a convenient tool for the application of transient gene expression. This model system has allowed the study of plant responses to biotic and abiotic stresses, protein location and trafficking, cell wall dynamics, and single-cell transcriptomics, among others. Although well-established protocols for isolating protoplasts from different plant tissues are available, they have never been used for studying plant cells using cryo electron microscopy (cryo-EM) and cryo electron tomography (cryo-ET). Here we describe a workflow to prepare root protoplasts from *Arabidopsis thaliana* plants for cryo-ET. The process includes protoplast isolation and vitrification on EM grids, and cryo-focused ion beam milling (cryo-FIB), with the aim of tilt series acquisition. The whole workflow, from growing the plants to the acquisition of the tilt series, may take a few months. Our protocol provides a novel application to use plant protoplasts as a tool for cryo-ET.

KEYWORDS

structural biology, *Arabidopsis thaliana*, protoplasts, cryo-EM, cryo-ET

Introduction

Understanding organelles' spatial distribution and macromolecules' cellular structure is fundamental to cell biology. Over the years, several techniques aiming to improve this understanding have been successfully applied to yeast and various mammalian cells, notably using electron cryo microscopy (cryo-EM) and cryo electron tomography (cryo-ET) approaches, which have provided unprecedented resolution (Oikonomou and Jensen, 2017; Pfeffer and Mahamid, 2018; Kühlbrandt, 2022; Young and Villa, 2023). Despite its many advances, applying EM techniques has been a challenge for plant biologists due to the thickness of plant tissues, cell and organelle size, presence of a cell wall, and preservation and subsequent handling of the sample for analysis (Otegui and Pennington, 2018; Liu et al., 2020). The visualization and localization of cellular components, organelle morphology, and analysis of individual structures have been possible thanks to the progress that light and electron microscopy approaches have undergone over the years

(Antony et al., 2013; Benjin and Ling, 2020; Cooper, 2000). On the one hand, fluorescence microscopy, with the use of a larger selection of better fluorophores, has made it possible to follow cellular processes and locate molecules of interest while imaging living cells. With its much higher spatial resolution, EM has allowed for studying different organisms at a much higher resolution, while obtaining information on cellular components that, combined with data from other methods, provides a valuable understanding of essential cellular processes (Cohen et al., 2002; O'Toole et al., 2002; Geimer and Melkonian, 2005; Herold et al., 2009; Kurth et al., 2010; Weiner et al., 2021; Kaplan et al., 2022).

Amongst the various EM approaches that can be applied to investigate biological specimens, cryo-EM has allowed scientists to visualize samples that are frozen-hydrated in their near-native (Murata and Wolf, 2018; Zhang, 2019). Therefore, through rapid freezing, it is possible to obtain structural preservation while maintaining the integrity of cells, organelles, and molecular assemblies (Beck and Baumeister, 2016). To study these frozen-hydrated samples, one of the structural determination methods that can be used is cryo-ET combined with subtomogram averaging (STA) (Wan and Briggs, 2016). Furthermore, it is necessary to consider that sample thickness represents a limiting factor for cryo-ET, effectively restricting this technique to samples thinner than 0.3–0.5 μm (Mahamid et al., 2015; Beck and Baumeister, 2016). To overcome this issue, vitrified specimens can be thinned using a focused ion beam microscope under cryogenic conditions (cryo-FIB) (Rigort and Plitzko, 2015). These methods together allow for achieving reconstructions that can reach sub-nanometer resolution (Wang et al., 2021; Zimmerli et al., 2021; Hoffmann et al., 2022; Lucas et al., 2022; Mosalaganti et al., 2022; Gemmer et al., 2023; Khavnekar et al., 2023).

While it has been possible to apply classical EM and ET techniques to study cellular plant processes (Reyes et al., 2011; Nicolas et al., 2017; Liang et al., 2018; Wang et al., 2019), few publications have shown that cryo-FIB milling and cryo-ET can be performed in plants and algae. The best-studied organism using these methods is *Chlamydomonas reinhardtii*, a small unicellular green alga, for which chloroplast architecture (Engel et al., 2015a), Golgi intracisternal protein arrays (Engel et al., 2015b), the native structure of COPI coats (Bykov et al., 2017), 26S proteasome complexes tethering to nuclear pore complexes (NPCs) (Albert et al., 2017), *in situ* structural studies of membrane proteins (Schaffer et al., 2017), *in situ* architecture of NPCs (Mosalaganti et al., 2018), centriole architecture (Klena et al., 2020), and thylakoid's individual protein complexes (Wietrzynski et al., 2020) have been revealed. More recently, cryo-FIB milling has been successfully applied using white onion (*Allium cepa*) epidermal cell wall peels to reveal the organization of cellulose fibers *in situ* (Nicolas et al., 2022). Likewise, cryo-lift-out in combination with cryo-ET have been employed effectively for studying tip-vesicles (TVs) in pollen tubes to better understand the function of TVs in pollen tubes (Liu et al., 2020). However, to date, the *in situ* use of cryo-FIB together with cryo-ET in vascular plant cells for revealing the structure of macromolecular assemblies and organelles in their near-native state in higher plants has not been achieved.

Here we describe a protocol for preparing plant protoplasts for cryo-FIB milling that enables the acquisition of tilt series. Plant protoplasts are isolated cells without cell walls (Yoo et al., 2007) that have been widely used as a versatile cell-based system to investigate plant cell reprogramming (Pasternak et al., 2020), transient and early events using transient expression systems (Yoo et al., 2007), screening of proteins involved to a specific abiotic (Chen et al., 2010; Wehner et al., 2011) or biotic stress (Asai et al., 2002; He et al., 2006; Boudsocq et al., 2010), auxin signaling and responses (Worley et al., 2000; Böttner et al., 2009), protein-protein interaction (Halter et al., 2014; Yeh et al., 2015; Gong et al., 2019; Ye et al., 2019), protein trafficking and localization (Asai et al., 2002; Ehlert et al., 2006; Underwood et al., 2017; Menzel et al., 2019), protoplast regeneration and plant breeding (Reed and Bargmann, 2021), and single-cell analysis (Efroni et al., 2015; Ryu et al., 2019; Xu et al., 2021; Zong et al., 2022), among others. Even if the protoplast isolation process involves eliminating the cell wall through an enzymatic process, it has been demonstrated that plant protoplasts retain their physiological responses, and original cellular and biochemical activities (Sheen, 2001; Yoo et al., 2007). While different protocols have been established for using protoplasts for various purposes, we describe the adaptations needed for *in situ* cryo-ET studies of plant macromolecules in their near-native. Our protocol details the steps necessary to obtain protoplasts from root tissue, to vitrify them on cryo-EM grids, and to target intact protoplasts for cryo-FIB lamellae preparation for cryo-ET. The protoplasts can in principle also be obtained from other tissues by adapting the protoplast isolation specifications. Lamellae preparation is performed by focused gallium ion beam milling, comparable to established protocols for other cell types (Schaffer et al., 2015; Wagner et al., 2020). The use of protoplasts, which are of a size consistent with the sample thickness required for cryo-FIB milling, and the fact that they can be properly vitrified makes this protocol suitable for tilt series acquisition and it could subsequently be used for sub-tomogram averaging.

Overview of the procedure

Before isolating protoplasts from Arabidopsis' roots, previously sterilized seeds should be grown in Murashige and Skoog Basal Medium (MS medium) with agar and Petri dishes must be placed vertically in the growth chamber. In this way, the plants will grow in a sterile manner, while the vertical position will cause the roots to grow at the surface of the growth media, allowing the user to have easy access to the roots once the plants are ready for use (Steps 1 and 2). After two weeks of growth, the roots can be easily cut and separated from the aerial part with a scalpel. Then, roots are immersed in the enzyme solution and cut into small pieces to start the digestion process of the plant cell wall (Steps 3–5). Once the digestion has been done, the isolated protoplasts must be filtered, spun, and washed for quantification and verification (Figure 1) (Steps 6–18) before proceeding to plunge freezing.

Plunge freezing (Steps 19–29) can be performed in liquid ethane with a plunger while adjusting the parameters according to the equipment's model and specifications. Next, the EM grids must be

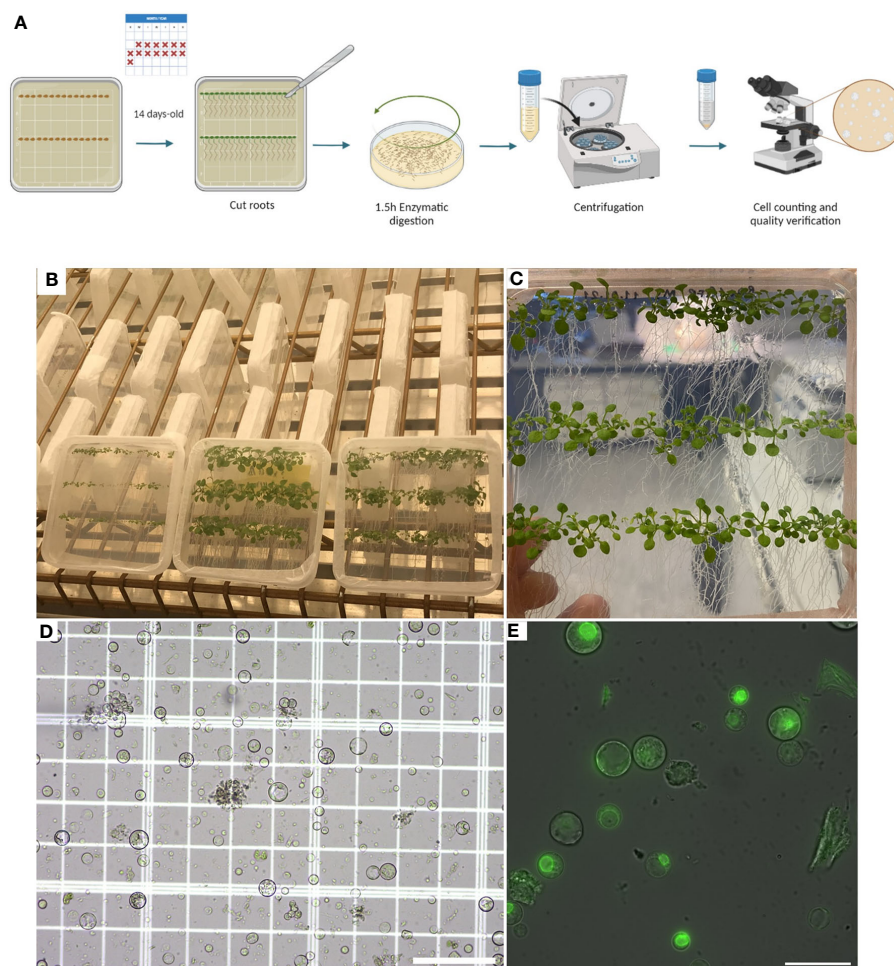


FIGURE 1

Plant growth and protoplast isolation (Steps 2–18). (A), Diagram describing the workflow from growing *Arabidopsis* plants in petri dishes containing MS media with agar for isolating and verifying root protoplasts under a microscope. (B), Photo showing how plants can be grown vertically for the roots to grow over the surface of the MS media with agar. (C), Photo of 14-day-old *Arabidopsis* plants expressing RAE1-GFP grown vertically. (D), Image of root protoplasts after digestion under a light microscope. (E), Confocal fluorescence image of root protoplasts expressing RAE1-GFP. Scale bars: 50 μm (D) and 25 μm (E).

clipped to continue with the workflow (Steps 30–39). Correlative Light and Electron Microscopy (CLEM) should be used to help identify intact protoplasts on the grids, and regions of interest that are labeled with a fluorophore using a light microscope fitted with a cryo-stage (Step 40–47) (Figure 2).

Once the target is identified, lamellae can be milled (Steps 48–56) from protoplasts on the EM grids in a dual-beam FIB/SEM microscope (Figure 3).

Finally, cryo-ET tilt series are acquired from these lamellae following established procedures (Steps 57–60) (Figure 4). Tomogram reconstruction was done using IMOD (Steps 61–64) and should be adjusted based on the needs and objectives of the respective study.

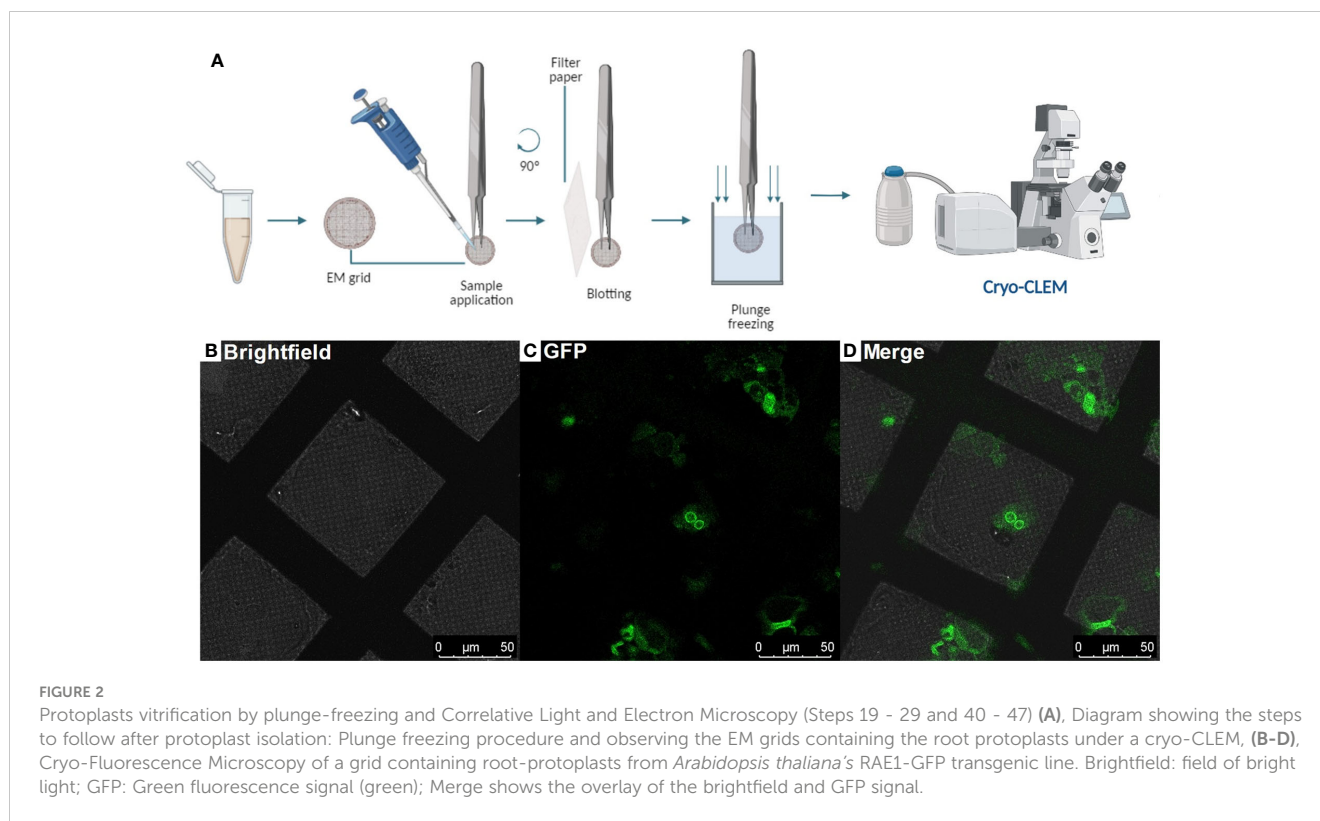
Level of expertise

The protocol presented here requires prior knowledge about growth conditions of *Arabidopsis thaliana*, as well as protoplast

handling and EM sample preparation at cryogenic temperatures. Thus, we presume that the researchers who would like to apply this workflow are familiar with light microscopy as well as cryo-ET sample preparation. Likewise, researchers should already be acquainted with the equipment and tools necessary to carry out the steps described here.

Applications of the method

This protocol describes a step-by-step procedure that allows the user to isolate plant protoplasts and prepare them for cryo-EM and cryo-ET. The application of *in situ* cryo-ET and its supplementary approaches to vascular plants was initially considered challenging due to their complexity and size (Otegui and Pennington, 2018; Liu et al., 2020). Our workflow introduces a possibility to carry out cryo-FIB sample preparation for cryo-ET studies on higher plants by using fresh plant protoplasts that can be obtained from different plant tissues and species.



This protocol can be applied to reveal the native structure of macromolecular complexes, proteins, and organelles in plant cells. To achieve this goal, modifications to this protocol could be made to expand its application.

Our protocol is strongly focused on the sample preparation of protoplasts for cryo-ET, we do not aim to describe reconstruction in detail. These steps can be performed with various software and protocols may vary depending on the scientific question asked. Nevertheless, we included these steps to give a complete picture from growing plants to analyzing data.

Comparison with other methods

This protocol was developed to apply cryo-ET approaches using plant protoplasts for the visualization of organelles and macromolecular complexes in their native environment. The application of the approaches mentioned in this protocol provides a new area of opportunity for *in situ* studies of complexes and organelles in plant cells. It is important to control the concentration of protoplasts to be plunge-frozen on a single EM grid. By taking care of this aspect, a density of protoplasts that can be analyzed is ensured, avoiding crystalline ice formation in thick samples that would harm molecular preservation. Other alternative methods have been used previously for the study and modeling of plant organelles. These alternatives include the application of cryo-immobilization under high pressure, followed by freeze-substitution (Austin et al., 2005; Otegui et al., 2006; Wilson and Bacic, 2012; Takeuchi et al., 2016; Cui et al., 2019), and more recently, the waffle method (Kelley et al.,

2022) which enables high-pressure freezing of thicker samples on grids for cryo-FIB milling. Although these approaches that do preserve native structures have provided valuable information about cellular structures in plants, some still use chemical fixatives and electron-dense stains to improve contrast, which are not compatible with native preservation needed for *in situ* structural biology. On the other hand, waffle and lift-out approaches usually require more experienced user interaction and more microscope time during sample preparation for their application.

In comparison, our protocol allows for the observation of frozen-hydrated samples close to their near native state without the use of chemicals or staining with heavy metals. Furthermore, it also offers the advantage of assessing protein structure inside plant protoplasts.

Advantages and limitations

The advantages of this protocol comprise the ability to prepare protoplasts from higher plants for cryo-EM and cryo-ET, while preserving the cellular structure. Among the advantages of our protocol, is the possibility to isolate protoplasts without requiring aseptic operations. This protocol can be easily implemented in almost any laboratory with access to a state-of-the-art EM facility. Similarly, it is possible to adapt the enzymatic solution for cell wall digestion, digestion time, sample to be used, and plunge freezing conditions and thus to apply this protocol to various plant sources. Another relevant point to consider is that in this work we used roots of *Arabidopsis thaliana* plants to obtain protoplasts. Therefore, it is essential to consider that we expected to have a heterogeneous

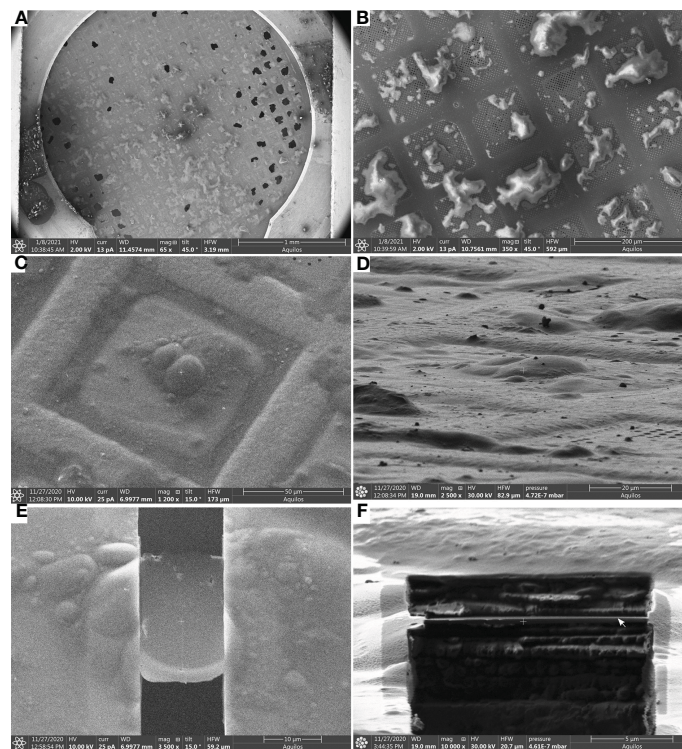


FIGURE 3
 Lamella milling (Steps 48-56) **(A)**, Scanning Electron Microscope (SEM) view of an EM grid containing vitrified root protoplasts from *Arabidopsis thaliana* RAE1-GFP transgenic line. **(B, C)**, SEM images (top view) of root protoplasts before milling. **(D)**, FIB view of root protoplasts. **(E)**, SEM view of a cryo-FIB milled lamella, and **(F)**, FIB view of a lamella. The lamella front in **(F)** is indicated by a white arrow. Scale bars: 1 mm **(a)**, 200 μm **(b)**, 50 μm **(c)**, 20 μm **(d)**, 10 μm **(E)**, and 5 μm **(F)**.

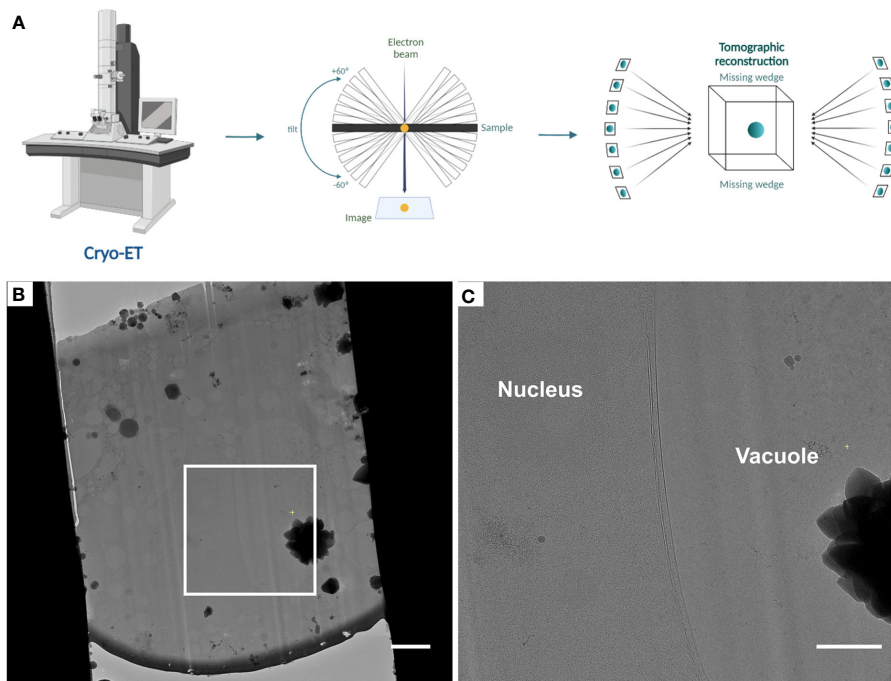


FIGURE 4
 Automated tomogram acquisition and tomogram reconstruction (Steps 57 - 64) **(A)**, Diagram representing the steps of tomogram acquisition and tomogram reconstruction. **(B)**, Cryo-TEM overview of lamellae after fine milling to a thickness of $\sim 180 - 200$ nm, the white box indicates the area shown in **(C)**. **(C)**, Higher magnification cryo-TEM overview. Scale bars: 2 μm **(B)** and 1 μm **(C)**.

population of cells. The heterogeneity of cell population could vary according to the type of organ used.

This workflow may present some disadvantages that should be considered before application. For example, while it is possible to find several efficient established protocols to successfully isolate protoplasts from model plants and crops, it is not feasible to isolate enough viable protoplasts from all organs and tissues of all plants due to species specificity constraints (Ren et al., 2021). However, the number of viable protoplasts on the grid directly affects EM grid quality as well as sample throughput and deviations of these parameters may make it difficult to obtain lamellae. Our protocol presents a powerful workflow for *in situ* structural studies of vascular plant cells, yet protoplasts are isolated cells outside of the context of tissue environment, which needs to be considered with respect to cell physiology and impact for the underlying cellular architecture.

MATERIALS:

REAGENTS

- Murashige and Skoog Basal Medium (Sigma-Aldrich, cat. no. M5519)
- Agar (Bio Basic, cat.no. FB0010)
- KOH (Millipore Sigma, cat. No. 105033)
- 0.2 M 4-morpholineethanesulfonic acid (MES, pH 5.7; FisherBiotech, cat. no. BP300)
- 0.8 M mannitol (Acros, cat. no.125340010)
- 1 M CaCl₂ (Bio Basic, cat. no. CT1330)
- 2 M KCl (Fisher scientific, cat. no. P330-500)
- 2 M MgCl₂ (Fisher Scientific, cat. no.M-20944)
- 154 mM NaCl (Fisher Scientific, cat. no. S271)
- Tris Base (Millipore Sigma, cat. no. 648310)
- HCl (Millipore Sigma, cat. no. 258148)
- β-Mercaptoethanol (Fisher Scientific, cat. no. BP176-100)
- BSA (Roche, cat. no. 10 735 086 001)
- Cellulase from (*Trichoderma* sp., Sigma-Aldrich, cat. no. C0615-1G)
- Pectinase from (*Aspergillus niger*, Sigma-Aldrich, cat. no. P4716)
- Concanavalin A (Sigma Aldrich, cat. no. C2010)
- Enzyme solution (see REAGENT SETUP)
- W5 solution (see REAGENT SETUP)

BIOLOGICAL MATERIALS

- *Arabidopsis* accessions: Col-0, RAE1-GFP (Tamura et al., 2010)

EQUIPMENT

- Square Petri Dishes (Fisher Scientific, cat no. FB0875711A)
- Sorvall Legend XFR Centrifuge (Thermo Fisher Scientific, cat. no. 75004541)
- 0.2-μm Syringe filter – Sterile (Fisher Scientific, cat. no. 09-719C)
- Sterile Single Use Carbon Blades (Lance, cat. no. 1500321)
- Petri dish with clear lid (Fisher Scientific, cat. no. FB0875712)
- Micropore (3M, cat. no. 1530-1)
- Sterile Cell Strainer 70 μm Nylon Mesh (Fisher Scientific, cat. no. 22-363-548)
- Improved Neubauer 0.1-mm-deep hemacytometer (Hausser Scientific, cat. no. 0267110)

- OMAX 40-2500X LED Digital Trinocular Compound Microscope USB Camera (OMAX, cat. No. M83EZ-SCP-C03S)
- Fluorescence microscope (Nikon microscope Ti2 Eclipse or comparable)
- 35 mm microscopy dishes, no. 1.5 Coverslip, 14 mm Glass Diameter, uncoated (Mattek)
- 2/1 Holey Carbon-coated SiO₂ 200-mesh Gold grids (Quantifoil Micro Tools GmbH, catalog number: Q2100CR1)
- Tweezers (Dumont 3, 5)
- Glass microscopy slides
- Glass Petri dishes
- Glow Discharge Cleaning System (PELCO easiGlow)
- Leica EM GP2 plunger (Leica Microsystems)
- Whatman filter paper grade 1
- Cryo grid boxes (custom-made) or (Thermo Fisher Scientific)
- Autogrids with FIB cutout (MPI Martinsried or Thermo Fisher Scientific)
- C-clips (Thermo Fisher Scientific)
- C-clip insertion tools (Thermo Fisher Scientific)
- EM Cryo CLEM system (Leica Microsystems)
- Aquilos Cryo-Focused Ion Beam - Scanning Electron Microscope (Thermo Fisher Scientific)
- Titan Krios G2 Cryo-Transmission Electron Microscope (Thermo Fisher Scientific), equipped with a BioQuantum-K3 (Gatan)

REAGENT SETUP

Enzyme solution:

Prepare a solution containing 0.4 M mannitol, 20 mM MES (pH 5.7), 20 mM KCl, 1.5% (wt/vol) cellulase, and 0.3% (wt/vol) macerozyme. Use 1 M Tris/HCl pH 7.5 to adjust the pH of the enzyme solution to 5.7. Warm the solution at 55°C for 10 minutes and cool to room temperature. Then, add 0.1% (wt/vol) of BSA, 10 mM of CaCl₂, and 5 mM of β-mercaptoethanol. The resulting enzyme solution should have a clear, light brown color. Pass the final enzyme solution through a 0.2 μm syringe filter into a Petri dish. Generally, 5 mL of enzyme solution can be used per 350 seedlings.

CRITICAL: The enzyme solution must be freshly made every time.

W5 solution:

Prepare a solution containing 154 mM NaCl, 125 mM CaCl₂, 5 mM KCl, and 2 mM MES (pH 5.7). The final W5 solution can be kept at room temperature.

PROCEDURE

Plant growth – Timing 2 weeks

1. Surface sterilize *Arabidopsis* seeds with 70% ethanol for 2 minutes, followed by 7% bleach and 0.1% Triton X-100 for 5 minutes. Then, wash the seeds 4 - 6 times with sterile water and stratify them in the dark for 48 hours at 4°C.

CRITICAL STEP: Prolonged exposition to ethanol or bleach during this step may affect seed germination.

2. In a biological safety cabinet, place seeds at a density of approximately 50 seeds per Petri box, in a straight line, over plant growth media consisting of ½ Murashige and Skoog Basal Medium supplemented with 1% agar and adjusted to pH 5.6-5.8 with KOH. Seal the Petri boxes using Micropore tape. Position the squared

Petri boxes vertically under a long-day photoperiod (16h of light, 8h of dark) at 23 °C, with an average light intensity of 120 mmol/m²/s⁻¹ at the level of the rosette.

CRITICAL STEP: the use of Micropore tape for sealing the Petri dishes keeps plates moist and sterile while allowing gas exchange.

Protoplast Isolation – Timing 2-3 hours

Protoplasts from roots were isolated according to the procedure of Bargmann, B. and Birnbaum, K (Au - Bargmann and Au - Birnbaum, 2010), with some modifications.

3. Harvest root tissue from Petri boxes containing 14-day-old plants with a scalpel and deposit them into the Petri dish containing 5 mL of enzyme solution.

4. Finely chop the roots until they are reduced into 1-2 mm pieces.

CRITICAL STEP: It is essential to cut the roots when they are in the solution and not when exposed to air, as they may dry out and further affect the quality and quantity of protoplasts.

5. Perform the enzymatic digestion from the chopped roots under agitation at 75 rpm for 1.5 h at room temperature.

CRITICAL STEP: Digestion time needs to be empirically optimized and relies on the experimental aims and desired responses.

6. After cell wall digestion, filter the solution through a 70 µm cell strainer nylon mesh into a new Falcon tube.

7. Add one volume of W5 solution, spin the protoplasts for 10 min at 500 x g, and then resuspend in cold W5 solution.

CRITICAL STEP: It is important to be gentle with protoplasts; however, handling them with regular pipette tips is possible.

8. For counting the protoplasts, place a glass cover slip over a Neubauer chamber (hemacytometer).

9. Using a pipette tip, gently mix the protoplast sample to ensure uniform cell dispersion.

10. Place the tip at the edge of the cover glass and use capillary action to the chambers of the Neubauer chamber.

11. Allow approximately one minute for the protoplasts to settle.

12. Examine each chamber at the proper magnification and count the number and quality of protoplasts in adequately sized grids.

13. The final protoplast concentration must be diluted to 500-650 protoplasts/µL in fresh W5 solution.

CRITICAL STEP: The concentration of protoplasts per µL may vary according to the cell type. However, it is essential to note that a very low or very high concentration of protoplasts per µL may not be optimal for the following steps.

? TROUBLESHOOTING

14. Use a wide-field fluorescence microscope to assess the fluorescence of the fluorophore-labeled target in the protoplasts.

15. Add 50 µL of Concanavalin A (concentration 1 mg/ml) to a clean glass-bottom dish to help immobilize the protoplasts while imaging them.

16. Let the Concanavalin A dry for 5 minutes.

17. Add a volume of 3µL diluted protoplasts and let protoplasts settle for 5 minutes before imaging.

18. Examine the protoplasts under the microscope for cell integrity.

Protoplasts vitrification by plunge-freezing – Timing 1 hour
Grid freezing is performed according to Schaffer, M., et al. (Schaffer et al., 2015), with some modifications.

19. Cool down the Plunge Freezer (Leica GP2) and set it to 70% humidity, chamber temperature of 23°C, single backside blotting, 6 sec blot time, and no delay before blotting.

CRITICAL STEP: Blotting parameters, such as blot time, as well as horizontal and vertical blot positions, need to be determined empirically, as they depend on the actual device used for Plunge Freezing.

20. Likewise, cool down the cryogen holder for liquid ethane, grid box reservoir, and first grid box to be used.

21. Take 200 mesh gold EM grids holey SiO₂ foil with tweezers and place them with the side of the foil on an objective glass slide.

22. Place the glass slide containing the EM grids over the Glow Discharge Cleaning System and glow discharge the grids for 90 s at 15 mA. Then, turn the EM grids facing the other side and glow discharge again for 90 s at 15 mA.

23. Store the slide containing the glow-discharged EM grids in a glass petri dish and proceed directly to plunge freezing the protoplasts.

24. Take one of the EM grids with tweezers and place it in blotting position.

25. Pipette 3 µL of diluted protoplasts onto the SiO₂ side of the EM grid inside the Plunge Freezer.

CRITICAL STEP: In our experience, the total amount of protoplasts present in 3 µL should be around 1500 to 2000. More or less quantity of cells may promote thick ice formation resulting in insufficient vitrification or not enough plunged protoplasts on the grids, respectively.

? TROUBLESHOOTING

26. Blot the grids from the back-side blotting for 6 sec.

27. Immediately plunge the EM grid containing the protoplasts into the liquid ethane reservoir at -183°C.

28. Then transfer it to the previously cooled-down grid box.

29. Repeat steps 19 to 28 with the rest of the EM grids and store the grid box(es) in a liquid nitrogen storage dewar.

PAUSE POINT: The frozen samples can now be stored in liquid nitrogen storage dewars.

CRITICAL STEP: A total of 8 - 12 EM grids containing protoplasts can be plunge frozen in 1 hour. On average, in our hands around 70% of all the plunge-frozen EM grids are suitable for the subsequent steps. However, this rate may vary according to protoplast concentration, EM grid material, and glow discharging and plunging conditions.

? TROUBLESHOOTING

Grid clipping – Timing approximately 1 h for about 10 EM grids

30. Once the protoplasts are plunged-frozen, EM grid clipping is carried out similar to a previous protocol of with the protocol of Schaffer, M., *et al.* (Schaffer et al., 2015).

31. Place the clipping support base into the loading box and fill it with clean liquid nitrogen.

32. Once the station has cooled down, transfer the cryo-grid box from the storage dewar to the loading box and open it there.

CRITICAL STEP: All transfer times should be kept as short as possible to avoid sample contamination.

CRITICAL STEP: All tools that will come into contact with the EM grids must be pre-cooled in liquid nitrogen in the loading box before usage.

33. Mark an AutoGrid with a fine point permanent marker prior clipping, 90° left and 90° right from the milling cut-out. The marks will additionally help to align the lamella sample in the cryo-FIB shuttle for cryo-FIB milling and then in the TEM cassette for cryo-ET.

34. Insert the marked AutoGrid with cryo-FIB cutout into one of the transfer pedestal's mounting positions.

35. Using a screw driver or comparable tool, loosen the top of the cryo-grid box.

36. Transfer the EM grid from the cryo-grid box and insert it in the Autogrid with the cell side and foil side facing down.

37. Using a loaded C-clip tool, clip the EM grid into the Autogrid with the C-clip.

38. Transfer the clipped EM grid back to the cryo-grid box.

39. Repeat steps 30 to 39 with all the EM grids.

CRITICAL STEP: Check for bent or damaged grids that are frequently unsuitable for cryo-CLEM or FIB milling and thus should be discarded at this stage.

Correlative Light and Electron Microscopy (CLEM) for cryo-ET – Timing approx. 1 h per grid.

40. After clipping the EM grids containing the plunge-frozen protoplasts, a fluorescence microscope fitted with a cryo-stage was used for identifying intact root protoplasts expressing RAE1-GFP, while discarding debris and broken/dead cells.

41. Cool down the machine according to the manufacturer's instructions.

42. Load the clipped EM grid into the cooled microscope

43. Start the software platform for image acquisition, select the proper acquisition parameters, and acquire a grid map overview image.

CRITICAL STEP: The parameters needed to locate the target of interest will depend on the type of fluorophore with which it is labeled.

44. Once having the grid map overview, choose and select potential target positions in individual squares.

45. Define and acquire focal-stacks of each of the selected grid squares.

46. The obtained fluorescent images containing the identified target of interest are used for targeted cryo-FIB milling.

Lamellae milling – Timing 8-10 hours, depending on the number of lamellae and sample quality. We usually made 8-10 lamellae during a 10-hour session.

A detailed protocol for loading the grid into the dual beam microscope has already been published (Wagner et al., 2020). Milling lamellae from EM grids is performed with an Aquilos

microscope as described previously (Schaffer et al., 2015; Hoffmann et al., 2022).

47. In brief, cool down the dual-beam microscope with liquid nitrogen and allow the stage to reach a temperature of ~ 183°C. The pressure in the microscope's chamber should be below 4×10^{-7} mbar.

48. Transfer EM grids into the microscope by loading them with pre-cooled tweezers into the shuttle. Make sure that the flat side of the Autogrid containing the protoplasts is facing outwards from the shuttle and orient the cut-out of the AutoGrid towards aligned with the ion beam.

49. Once loaded, check the grids with the SEM at a low current.

50. With the gas injection system (GIS), coat the samples with a layer of organometallic platinum for 10 s.

51. Then, sputter coat the samples with platinum for 10 s at voltage 1kV voltage and 10 mA current.

52. Move to the mapping positions and identify appropriate protoplasts for lamellae milling. Fluorescence data from steps 40-47 can be used as guidance to identify the position of intact protoplasts, which can sometimes be hard to distinguish on the EM grid alone.

CRITICAL STEP: For compatibility with cryo-ET later, choose lamellae milling areas that are within 5-6 grid squares from the center of the grid and within the center of individual grid squares.

53. Once the appropriate milling areas are identified, tilt the stage to a milling position of 15°, corresponding to a lamella angle of 8° in respect to the grid. Begin milling the lamellae in a step-wise fashion, by gradually decreasing the ion beam current from 1 nA, 500 pA, 300 pA and 100 pA.

54. Carry out final polishing of the lamellae with 50 pA to obtain a final thickness between ~180-200 nm of biological material.

55. After polishing, add an optional final sputter layer with platinum for 1-2 s at 1 kV and 10 mA.

PAUSE POINT: The frozen samples can be stored in liquid nitrogen in their respective storage dewar until imaged by cryo-TEM.

The following steps are added for completeness. Note that the focus of this protocol is the sample preparation. Cryo-ET acquisition and tomogram reconstruction may vary depending on the software, acquisition scheme used and for different scientific questions.

Automated tomogram acquisition – Timing can vary from hours to days, depending on the number of EM grids and lamellae to be observed, typically we use 2-4 grids for a 48 hr microscope session.

When the desired quantity of milled lamellae is obtained from different EM grids containing plunge-frozen protoplasts, tilt series acquisition can be conducted as described previously (Wagner et al., 2020).

56. Briefly, load EM grids containing milled lamellae into the Autoloader cassette so that the mark on the rim of the EM grid is centered in a 90° top-down view, keeping the grids in this position.

57. Load the Autoloader containing the EM grids into the TEM microscope under cryogenic conditions. The marks on the Autogrid help to manually align the grid during loading into the cassette. The cutout should face sideways when loading the cassette.

CRITICAL STEP: Check the Autogrid orientation to ensure that milling direction of the lamellae are rotated perpendicular

to microscope tilt axis. This will ensure access to the areas of interest at high tilt and optimal sample movement when tilting.

59. Find the lamellae for each EM grid at low magnification and take montaged overview images of the lamellae.

60. Determine the pre-tilt from the lamella orientation and using SerialEM software begin the tilt series acquisition under low-dose conditions.

Tomogram reconstruction – Timing can vary depending on the quantity of data acquired.

Tomogram reconstruction can be performed with adequately established software. We used patch-tracking from IMOD as previously described (Hoffmann et al., 2022).

61. Briefly, pre-process the tilt series by performing dose-filtering using MATLAB (Wan et al., 2017).

62. Remove poor-quality tilt images (if any) from the tilt series.

63. Using eTomo (IMOD, versions 4.11.5), align the dose-filtered tilt series with the patch-tracking alignment method (Mastrorade and Held, 2017).

64. For tomogram generation for visualization purposes, reconstruct back-projected tomograms with SIRT-like filtering.

Anticipated results

Performing the protocol described here will allow the user to prepare and obtain lamellae appropriate for cryo-ET acquisition (results shown in Figure 5). Therefore use of protoplasts represents a valuable tool for studying organellar and macromolecular structures in plant cells.

Troubleshooting

Troubleshooting advice can be found in Table 1.

TIMING

Steps 1-2: 2 weeks

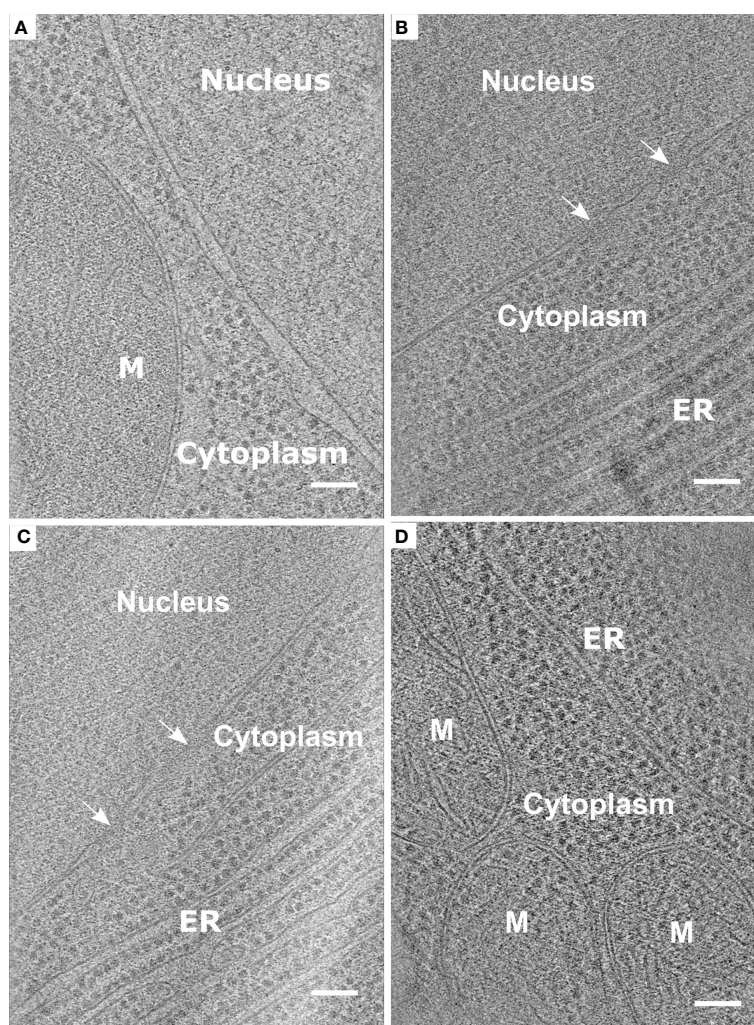


FIGURE 5

Representative data obtained from the protocol described using root protoplasts from *Arabidopsis thaliana*. (A–D). Slices through tomograms taken from vitrified and milled root protoplasts (lamella thickness: ~ 200 nm or less). Slices through the tomograms show mitochondria (M), Endoplasmic reticulum (ER), and Nuclear Pore Complexes (white arrows). Scale bars: 100 nm (A–D).

TABLE 1 Troubleshooting table.

Step	Problem	Possible reason	Solution
13	Poor/bad quality protoplast yield	Poor plant growth conditions	Check that the pH of the MS media is between 5.6-5.8. Check and optimize growth conditions, such as light intensity, temperature, and photoperiod.
		Ineffective enzymatic digestion	Optimize digestion time for each transgenic line, accession, and plant tissue.
25	The protoplasts do not adhere properly	Insufficient glow discharging	Verify and adapt glow discharge conditions.
29	Non-vitrified ice in the samples	Many cells were not properly plunge frozen, producing a thick sample	Adjust the number of protoplasts when plunge freezing.
		Poor blotting conditions	Adjust the blotting parameters adequately, depending on the type of filter paper to be used, as well as the blotting force and time.

Steps 3-18: approximately 2 – 3 h

Steps 19-29: approximately 1 h

Steps 30-39: approximately 1 h

Steps 40-47: approximately 1 h per grid

Steps 48-56: approximately 8 – 10 h

Steps 57-60: variable timing

Steps 61-64: variable timing

Acknowledgments

We thank Mark Linder, Sonja Welsch, and the team from the Electron Microscopy Facility at the Max-Planck-Institute for Biophysics for support with data acquisition; as well as to all the members of the Molecular Sociology Department for input. Schematics of the workflow (Figures 1A, 2A, 4A) were created with Biorender.com.

Data availability statement

The original contributions presented in the study are included in the article/Supplementary Material. Further inquiries can be directed to the corresponding author.

Author contributions

IS: Conceptualization, Formal Analysis, Investigation, Methodology, Writing – original draft, Writing – review & editing. PH: Conceptualization, Data curation, Formal Analysis, Investigation, Methodology, Writing – review & editing, Funding acquisition. TB: Conceptualization, Investigation, Writing – original draft. MB: Conceptualization, Project administration, Resources, Supervision, Writing – review & editing. HG: Conceptualization, Funding acquisition, Investigation, Project administration, Resources, Supervision, Writing – review & editing.

Funding

This project was supported by the Globalink Research Award, the Max-Planck-Institute for Biophysics, and the International Relations Office from the Université du Québec à Trois Rivières. PH is supported by an EMBO Postdoctoral Fellowship (ALTF-33-2021).

Conflict of interest

The authors declare that the research was conducted in the absence of any commercial or financial relationships that could be construed as a potential conflict of interest.

Publisher's note

All claims expressed in this article are solely those of the authors and do not necessarily represent those of their affiliated organizations, or those of the publisher, the editors and the reviewers. Any product that may be evaluated in this article, or claim that may be made by its manufacturer, is not guaranteed or endorsed by the publisher.

Supplementary material

The Supplementary Material for this article can be found online at: <https://www.frontiersin.org/articles/10.3389/fpls.2023.1261180/full#supplementary-material>

SUPPLEMENTARY VIDEO 1

Tomogram showing data obtained from *Arabidopsis* protoplasts. Tomogram taken from vitrified and milled root protoplasts (lamella thickness: ~ 200 nm or less). The tomogram shows mitochondria through the slices. Scale bar is 200nm.

References

- Albert, S., Schaffer, M., Beck, F., Mosalaganti, S., Asano, S., Thomas, H. F., et al. (2017). Proteasomes tether to two distinct sites at the nuclear pore complex. *Proc. Natl. Acad. Sci.* 114, 13726–13731. doi: 10.1073/pnas.1716305114
- Antony, P. P. M. A., Trefois, C., Stojanovic, A., Baumuratov, A. S., and Kozak, K. (2013). Light microscopy applications in systems biology: opportunities and challenges. *Cell Communication Signaling* 11, 24. doi: 10.1186/1478-811X-11-24
- Asai, T., Tena, G., Plotnikova, J., Willmann, M. R., Chiu, W.-L., Gomez-Gomez, L., et al. (2002). MAP kinase signalling cascade in Arabidopsis innate immunity. *Nature* 415, 977–983. doi: 10.1038/415977a
- Au - Bargmann, B. O. R., and Au - Birnbaum, K. D. (2010). Fluorescence activated cell sorting of plant protoplasts. *JoVE* 18 (36), 1673. doi: 10.3791/1673
- Austin, J. R. II, Seguí-Simarro, J. M., and Staehelin, L. A. (2005). Quantitative analysis of changes in spatial distribution and plus-end geometry of microtubules involved in plant-cell cytokinesis. *J. Cell Sci.* 118, 3895–3903. doi: 10.1242/jcs.02512
- Beck, M., and Baumeister, W. (2016). Cryo-electron tomography: can it reveal the molecular sociology of cells in atomic detail? *Trends Cell Biol.* 26, 825–837. doi: 10.1016/j.tcb.2016.08.006
- Benjin, X., and Ling, L. (2020). Developments, applications, and prospects of cryo-electron microscopy. *Protein Sci.* 29, 872–882. doi: 10.1002/pro.3805
- Böttner, S., Iven, T., Carsjens, C. S., and Dröge-Laser, W. (2009). Nuclear accumulation of the ankyrin repeat protein ANK1 enhances the auxin-mediated transcription accomplished by the bZIP transcription factors BZI-1 and BZI-2. *Plant J.* 58, 914–926. doi: 10.1111/j.1365-313X.2009.03829.x
- Boudsocq, M., Willmann, M. R., McCormack, M., Lee, H., Shan, L., He, P., et al. (2010). Differential innate immune signalling via Ca²⁺ sensor protein kinases. *Nature* 464, 418–422. doi: 10.1038/nature08794
- Bykov, Y. S., Schaffer, M., Dodonova, S. O., Albert, S., Plitzko, J. M., Baumeister, W., et al. (2017). The structure of the COPI coat determined within the cell. *eLife* 6, e32493. doi: 10.7554/eLife.32493
- Chen, H., Lai, Z., Shi, J., Xiao, Y., Chen, Z., and Xu, X. (2010). Roles of arabidopsis WRKY18, WRKY40 and WRKY60 transcription factors in plant responses to abscisic acid and abiotic stress. *BMC Plant Biol.* 10, 281. doi: 10.1186/1471-2229-10-281
- Cohen, M., Tzur, Y. B., Neufeld, E., Feinstein, N., Delannoy, M. R., Wilson, K. L., et al. (2002). Transmission electron microscope studies of the nuclear envelope in *Caenorhabditis elegans* embryos. *J. Struct. Biol.* 140, 232–240. doi: 10.1016/S1047-8477(02)00516-6
- Cooper, G. M. (2000). *The Cell: A Molecular Approach. 2nd edition* (ed Sunderland) Ch. The Origin and Evolution of Cells. (Washington, D.C.: Sinauer Associates).
- Cui, Y., Cao, W., He, Y., Zhao, Q., Wakazaki, M., Zhuang, X., et al. (2019). A whole-cell electron tomography model of vacuole biogenesis in Arabidopsis root cells. *Nat. Plants* 5, 95–105. doi: 10.1038/s41477-018-0328-1
- Efroni, I., Ip, P.-L., Nawy, T., Mello, A., and Birnbaum, K. D. (2015). Quantification of cell identity from single-cell gene expression profiles. *Genome Biol.* 16, 9. doi: 10.1186/s13059-015-0580-x
- Ehler, A., Weltmeier, F., Wang, X., Mayer, C. S., Smeekens, S., Vicente-Carabajosa, J., et al. (2006). Two-hybrid protein–protein interaction analysis in Arabidopsis protoplasts: establishment of a heterodimerization map of group C and group S bZIP transcription factors. *Plant J.* 46, 890–900. doi: 10.1111/j.1365-313X.2006.02731.x
- Engel, B. D., Schaffer, M., Kuhn Cuellar, L., Villa, E., Plitzko, J. M., and Baumeister, W. (2015a). Native architecture of the *Chlamydomonas* chloroplast revealed by *in situ* cryo-electron tomography. *eLife* 4, e04889. doi: 10.7554/eLife.04889
- Engel, B. D., Schaffer, M., Albert, S., Asano, S., Plitzko, J. M., and Baumeister, W. (2015b). *In situ* structural analysis of Golgi intracisternal protein arrays. *Proc. Natl. Acad. Sci.* 112, 11264–11269. doi: 10.1073/pnas.1515337112
- Geimer, S., and Melkonian, M. (2005). Centrin scaffold in *chlamydomonas reinhardtii* revealed by immunoelectron microscopy. *Eukaryotic Cell* 4, 1253–1263. doi: 10.1128/EC.4.7.1253-1263.2005
- Gemmer, M., Chaillet, M. L., van Loenhout, J., Cuevas Arenas, R., Vismpas, D., Gröllers-Mulderij, M., et al. (2023). Visualization of translation and protein biogenesis at the ER membrane. *Nature* 614, 160–167. doi: 10.1038/s41586-022-05638-5
- Gong, B.-Q., Guo, J., Zhang, N., Yao, X., Wang, H.-B., and Li, J.-F. (2019). Cross-Microbial Protection via Priming a Conserved Immune Co-Receptor through Juxtamembrane Phosphorylation in Plants. *Cell Host Microbe* 26, 810–822.e817. doi: 10.1016/j.chom.2019.10.010
- Halter, T., Imkamp, J., Mazzotta, S., Wierzbza, M., Postel, S., Bücherl, C., et al. (2014). The leucine-rich repeat receptor kinase BIR2 is a negative regulator of BAK1 in plant immunity. *Curr. Biol.* 24, 134–143. doi: 10.1016/j.cub.2013.11.047
- He, P., Shan, L., Lin, N.-C., Martin, G. B., Kemmerling, B., Nürnberger, T., et al. (2006). Specific bacterial suppressors of MAMP signaling upstream of MAPKKK in Arabidopsis Innate Immunity Cell 125, 563–575. doi: 10.1016/j.cell.2006.02.047
- Herold, N., Will, C. L., Wolf, E., Kastner, B., Urlaub, H., and Lührmann, R. (2009). Conservation of the protein composition and electron microscopy structure of drosophila melanogaster and human spliceosomal complexes. *Mol. Cell Biol.* 29, 281–301. doi: 10.1128/MCB.01415-08
- Hoffmann, P. C., Kreysing, J. P., Khusainov, I., Tuijtel, M. W., Welsch, S., and Beck, M. (2022). Structures of the eukaryotic ribosome and its translational states *in situ*. *Nat. Commun.* 13, 7435. doi: 10.1038/s41467-022-34997-w
- Kaplan, M., Oikonomou, C. M., Wood, C. R., Chreifi, G., Ghosal, D., Dobro, M. J., et al. (2022). Discovery of a novel inner membrane-associated bacterial structure related to the flagellar type III secretion system. *J. Bacteriology* 204, e00144–e00122. doi: 10.1128/jb.00144-22
- Kelley, K., Raczkowski, A. M., Klykov, O., Jaroenlak, P., Bobe, D., Kopylov, M., et al. (2022). Waffle Method: A general and flexible approach for improving throughput in FIB-milling. *Nat. Commun.* 13, 1857. doi: 10.1038/s41467-022-29501-3
- Khavnekar, S., Wan, W., Majumder, P., Wietrzynski, W., Erdmann, P. S., and Plitzko, J. M. (2023). Multishot tomography for high-resolution *in situ* subtomogram averaging. *J. Struct. Biol.* 215, 107911. doi: 10.1016/j.jsb.2022.107911
- Klena, N., Le Guennec, M., Tassin, A.-M., van den Hoek, H., Erdmann, P. S., Schaffer, M., et al. (2020). Architecture of the centriole cartwheel-containing region revealed by cryo-electron tomography. *EMBO J.* 39, e106246. doi: 10.15252/embj.2020106246
- Kühlbrandt, W. (2022). Forty years in cryoEM of membrane proteins. *Microscopy* 71, i30–i50. doi: 10.1093/jmicro/dfab041
- Kurth, T., Berger, J., Wilsch-Bräuninger, M., Kretschmar, S., Cerny, R., Schwarz, H., et al. (2010). *Methods in Cell Biology* Vol. 96. Ed. T. Müller-Reichert (London: Academic Press), 395–423.
- Liang, Z., Zhu, N., Mai, K. K., Liu, Z., Tzeng, D., Osteryoung, K. W., et al. (2018). Thylakoid-bound polysomes and a dynamin-related protein, FZL, mediate critical stages of the linear chloroplast biogenesis program in greening arabidopsis cotyledons. *Plant Cell* 30, 1476–1495. doi: 10.1105/tpc.17.00972
- Liu, Z., Gao, J., Cui, Y., Klumpe, S., Xiang, Y., Erdmann, P. S., et al. (2020). Membrane imaging in the plant endomembrane system. *Plant Physiol.* 185, 562–576. doi: 10.1093/plphys/kiaa040
- Lucas, B. A., Zhang, K., Loerch, S., and Grigorieff, N. (2022). *In situ* single particle classification reveals distinct 60S maturation intermediates in cells. *eLife* 11, e79272. doi: 10.7554/eLife.79272
- Mahamid, J., Schampers, R., Persoon, H., Hyman, A. A., Baumeister, W., and Plitzko, J. M. (2015). A focused ion beam milling and lift-out approach for site-specific preparation of frozen-hydrated lamellas from multicellular organisms. *J. Struct. Biol.* 192, 262–269. doi: 10.1016/j.jsb.2015.07.012
- Mastronarde, D. N., and Held, S. R. (2017). Automated tilt series alignment and tomographic reconstruction in IMOD. *J. Struct. Biol.* 197, 102–113. doi: 10.1016/j.jsb.2016.07.011
- Menzel, W., Stenzel, I., Helbig, L.-M., Krishnamoorthy, P., Neumann, S., Eschen-Lippold, L., et al. (2019). A PAMP-triggered MAPK cascade inhibits phosphatidylinositol 4,5-bisphosphate production by PIP5K6 in Arabidopsis thaliana. *New Phytol.* 224, 833–847. doi: 10.1111/nph.16069
- Mosalaganti, S., Kosinski, J., Albert, S., Schaffer, M., Strenkert, D., Salomé, P. A., et al. (2018). *In situ* architecture of the algal nuclear pore complex. *Nat. Commun.* 9, 2361. doi: 10.1038/s41467-018-04739-y
- Mosalaganti, S., Obarska-Kosinska, A., Siggel, M., Taniguchi, R., Turoňová, B., Zimmerli, C. E., et al. (2022). AI-based structure prediction empowers integrative structural analysis of human nuclear pores. *Science* 376, eabm9506. doi: 10.1126/science.abm9506
- Murata, K., and Wolf, M. (2018). Cryo-electron microscopy for structural analysis of dynamic biological macromolecules. *Biochim. Biophys. Acta (BBA) - Gen. Subj.* 1862, 324–334. doi: 10.1016/j.bbagen.2017.07.020
- Nicolas, W. J., Grison, M. S., Tréput, S., Gaston, A., Fouché, M., Cordelières, K., et al. (2017). Architecture and permeability of post-cytokinesis plasmodesmata lacking cytoplasmic sleeves. *Nat. Plants* 3, 17082. doi: 10.1038/nplants.2017.82
- Nicolas, W. J., et al. (2022). Cryo-electron tomography of the onion cell wall shows bimodally oriented cellulose fibers and reticulated homogalacturonan networks. *Curr. Biol.* 32, 2375–2389.e2376. doi: 10.1016/j.cub.2022.04.024
- O’Toole, E. T., Winey, M., McIntosh, J. R., and Mastronarde, D. N. (2002). Electron tomography of yeast cells. *Methods Enzymol.* 351, 81–95. doi: 10.1016/s0076-6879(02)51842-5
- Oikonomou, C. M., and Jensen, G. J. (2017). Cellular electron cryotomography: toward structural biology *in situ*. *Annu. Rev. Biochem.* 86, 873–896. doi: 10.1146/annurev-biochem-061516-044741
- Otegui, M. S., Herder, R., Schulze, J., Jung, R., and Staehelin, L. A. (2006). The proteolytic processing of seed storage proteins in Arabidopsis embryo cells starts in the multivesicular bodies. *Plant Cell* 18, 2567–2581. doi: 10.1105/tpc.106.040931
- Otegui, M. S., and Pennington, J. G. (2018). Electron tomography in plant cell biology. *Microscopy* 68, 69–79. doi: 10.1093/jmicro/dfy133
- Pasternak, T., Lystvan, K., Betekhtin, A., and Hasterok, R. (2020). From single cell to plants: mesophyll protoplasts as a versatile system for investigating plant cell reprogramming. *Int. J. Mol. Sci.* 21. doi: 10.3390/ijms21124195
- Pfeffer, S., and Mahamid, J. (2018). Unravelling molecular complexity in structural cell biology. *Curr. Opin. Struct. Biol.* 52, 111–118. doi: 10.1016/j.sbi.2018.08.009

- Reed, K. M., and Bargmann, B. O. R. (2021). Protoplast regeneration and its use in new plant breeding technologies. *Front. Genome Editing* 3. doi: 10.3389/fgeed.2021.734951
- Ren, R., Gao, J., Yin, D., Li, K., Lu, C., Ahmad, S., et al. (2021). Highly efficient leaf base protoplast isolation and transient expression systems for orchids and other important monocot crops. *Front. Plant Sci.* 12. doi: 10.3389/fpls.2021.626015
- Reyes, F., Chung, T., Holding, D., Jung, R., Vierstra, R., and Otegui, M. (2011). Delivery of prolamins to the protein storage vacuole in maize aleurone cells. *Plant Cell* 23, 769–784. doi: 10.1105/tpc.110.082156
- Rigort, A., and Plitzko, J. M. (2015). Cryo-focused-ion-beam applications in structural biology. *Arch. Biochem. Biophys.* 581, 122–130. doi: 10.1016/j.abb.2015.02.009
- Ryu, K. H., Huang, L., Kang, H. M., and Schiefelbein, J. (2019). Single-cell RNA sequencing resolves molecular relationships among individual plant cells. *Plant Physiol.* 179, 1444. doi: 10.1104/pp.18.01482
- Schaffer, M., Engel, B. D., Laugks, T., Mahamid, J., Plitzko, J. M., and Baumeister, W. (2015). Cryo-focused ion beam sample preparation for imaging vitreous cells by cryo-electron tomography. *Bio-protocol* 5, e1575. doi: 10.21769/BioProtoc.1575
- Schaffer, M., Mahamid, J., Engel, B., Laugks, T., Baumeister, W., and Plitzko, J. (2017). Optimized cryo-focused ion beam sample preparation aimed at *in situ* structural studies of membrane proteins. *J. Struct. Biol.* 197, 73–82. doi: 10.1016/j.jsb.2016.07.010
- Sheen, J. (2001). Signal transduction in maize and Arabidopsis mesophyll protoplasts. *Plant Physiol.* 127, 1466–1475. doi: 10.1104/pp.010820
- Takeuchi, M., Karahara, I., Kajimura, N., Takaoka, A., Murata, K., Misaki, K., et al. (2016). Single microfilaments mediate the early steps of microtubule bundling during preprophase band formation in onion cotyledon epidermal cells. *Mol. Biol. Cell* 27, 1809–1820. doi: 10.1091/mbc.E15-12-0820
- Tamura, K., Fukao, Y., Iwamoto, M., Haraguchi, T., and Hara-Nishimura, I. (2010). Identification and characterization of nuclear pore complex components in *Arabidopsis thaliana*. *Plant Cell* 22, 4084. doi: 10.1105/tpc.110.079947
- Underwood, W., Ryan, A., and Somerville, S. C. (2017). An Arabidopsis lipid flippase is required for timely recruitment of defenses to the host–pathogen interface at the plant cell surface. *Mol. Plant* 10, 805–820. doi: 10.1016/j.molp.2017.04.003
- Wagner, F. R., Watanabe, R., Schampers, R., Singh, D., Persoon, H., Schaffer, M., et al. (2020). Preparing samples from whole cells using focused-ion-beam milling for cryo-electron tomography. *Nat. Protoc.* 15, 2041–2070. doi: 10.1038/s41596-020-0320-x
- Wan, W., and Briggs, J. A. G. (2016). *Methods in Enzymology* Vol. 579. Ed. R. A. Crowther (New York: Academic Press), 329–367.
- Wan, W., Kolesnikova, L., Clarke, M., Koehler, A., Noda, T., Becker, S., et al. (2017). Structure and assembly of the Ebola virus nucleocapsid. *Nature* 551, 394–397. doi: 10.1038/nature24490
- Wang, Z., Grange, M., Wagner, T., Kho, A. L., Gautel, M., and Raunser, S. (2021). The molecular basis for sarcomere organization in vertebrate skeletal muscle. *Cell* 184, 2135–2150.e2113. doi: 10.1016/j.cell.2021.02.047
- Wang, P., Liang, Z., and Kang, B.-H. (2019). Electron tomography of plant organelles and the outlook for correlative microscopic approaches. *New Phytol.* 223, 1756–1761. doi: 10.1111/nph.15882
- Wehner, N., Hartmann, L., Ehlert, A., Böttner, S., Oñate-Sánchez, L., and Dröge-Laser, W. (2011). High-throughput protoplast transactivation (PTA) system for the analysis of Arabidopsis transcription factor function. *Plant J.* 68, 560–569. doi: 10.1111/j.1365-3113X.2011.04704.x
- Weiner, E., Pinskey, J. M., Nicastro, D., and Otegui, M. S. (2021). Electron microscopy for imaging organelles in plants and algae. *Plant Physiol.* 188, 713–725. doi: 10.1093/plphys/kiab449
- Wietrzynski, W., Schaffer, M., Tegunov, D., Albert, S., Kanazawa, A., Plitzko, J. M., et al. (2020). Charting the native architecture of Chlamydomonas thylakoid membranes with single-molecule precision. *eLife* 9, e53740. doi: 10.7554/eLife.53740
- Wilson, S. M., and Bacic, A. (2012). Preparation of plant cells for transmission electron microscopy to optimize immunogold labeling of carbohydrate and protein epitopes. *Nat. Protoc.* 7, 1716–1727. doi: 10.1038/nprot.2012.096
- Worley, C. K., Zenser, N., Ramos, J., Rouse, D., Leyser, O., Theologis, A., et al. (2000). Degradation of Aux/IAA proteins is essential for normal auxin signalling. *Plant J.* 21, 553–562. doi: 10.1046/j.1365-313x.2000.00703.x
- Xu, X., Crow, M., Rice, B. R., Li, F., Harris, B., Liu, L., et al. (2021). Single-cell RNA sequencing of developing maize ears facilitates functional analysis and trait candidate gene discovery. *Dev. Cell* 56, 557–568.e556. doi: 10.1016/j.devcel.2020.12.015
- Ye, K., Li, H., Ding, Y., Shi, Y., Song, C., Gong, Z., et al. (2019). BRASSINOSTEROID-INSENSITIVE2 negatively regulates the stability of transcription factor ICE1 in response to cold stress in Arabidopsis. *Plant Cell* 31, 2682–2696. doi: 10.1105/tpc.19.00058
- Yeh, Y.-H., Chang, Y.-H., Huang, P.-Y., Huang, J.-B., and Zimmerli, L. (2015). Enhanced Arabidopsis pattern-triggered immunity by overexpression of cysteine-rich receptor-like kinases. *Front. Plant Sci.* 6. doi: 10.3389/fpls.2015.00322
- Yoo, S.-D., Cho, Y.-H., and Sheen, J. (2007). Arabidopsis mesophyll protoplasts: a versatile cell system for transient gene expression analysis. *Nat. Protoc.* 2, 1565–1572. doi: 10.1038/nprot.2007.199
- Young, L. N., and Villa, E. (2023). Bringing structure to cell biology with cryo-electron tomography. *Annu. Rev. Biophys.* 52, 573–595. doi: 10.1146/annurev-biophys-111622-091327
- Zhang, P. (2019). Advances in cryo-electron tomography and subtomogram averaging and classification. *Curr. Opin. Struct. Biol.* 58, 249–258. doi: 10.1016/j.sbi.2019.05.021
- Zimmerli, C. E., Allegretti, M., Rantos, V., Goetz, S. K., Obarska-Kosinska, A., Zagoriy, I., et al. (2021). Nuclear pores dilate and constrict in cellulose. *Science* 374, eabd9776. doi: 10.1126/science.abd9776
- Zong, J., Wang, L., Zhu, L., Bian, L., Zhang, B., Chen, X., et al. (2022). A rice single cell transcriptomic atlas defines the developmental trajectories of rice floret and inflorescence meristems. *New Phytol.* 234, 494–512. doi: 10.1111/nph.18008